Virus Research 244 (2018) 53–63

Contents lists available at ScienceDirect

Virus Research

journal homepage: www.elsevier.com/locate/virusres

Quantifying rotavirus kinetics in the REH tumor cell line using in vitro data

Gilberto González-Parra[a,b], Hana M. Dobrovolny[b,*], Diego F. Aranda[c], Benito Chen-Charpentier[d], Rafael Antonio Guerrero Rojas[e]

[a] Department of Physics and Astronomy, Texas Christian University, Fort Worth, TX, USA
[b] Department of Mathematics, New Mexico Tech, Socorro, NM, USA
[c] Facultad de Ciencias, Departamento de Matemáticas, Universidad El Bosque, Bogotá D.C., Colombia
[d] Department of Mathematics, University of Texas at Arlington, TX, USA
[e] Grupo de Biología Molecular del Virus, Universidad Nacional de Colombia, Bogotá D.C., Colombia

ARTICLE INFO

Keywords:
Rotavirus
Mathematical model
Oncolytic virus
Eclipse
Infectious lifespan

ABSTRACT

Globally, rotavirus is the most common cause of diarrhea in children younger than 5 years of age, however, a quantitative understanding of the infection dynamics is still lacking. In this paper, we present the first study to extract viral kinetic parameters for *in vitro* rotavirus infections in the REH cell tumor line. We use a mathematical model of viral kinetics to extract parameter values by fitting the model to data from rotavirus infection of REH cells. While accurate results for some of the parameters of the mathematical model were not achievable due to its global non-identifiability, we are able to quantify approximately the time course of the infection for the first time. We also find that the basic reproductive number of rotavirus, which gives the number of secondary infections from a single infected cell, is much greater than one. Quantifying the kinetics of rotavirus leads not only to a better understanding of the infection process, but also provides a method for quantitative comparison of kinetics of different strains or for quantifying the effectiveness of antiviral treatment.

1. Introduction

Diarrhea is one of the leading causes of mortality among children under five years old worldwide (Black et al., 2010). Rotaviruses are the single most important agents of diarrhea associated with mortality in this age group (Bruun et al., 2016; Ho et al., 1988). While there is a rotavirus vaccine that has mitigated some of the disease burden in wealthy countries (Gervasi et al., 2016; Prelog et al., 2016; Lamberti et al., 2016), rotavirus still creates a heavy burden in low income countries (Bennett et al., 2016; Mehendale et al., 2016; Lamberti et al., 2016). Issues such as low vaccine coverage and low on-time immunization in developing countries limit the benefits of vaccination (Guerrero et al., 2013; Santosham, 2010). Thus, there is still a need to develop strategies for treating rotavirus-associated diarrhea, especially in the poorest countries (Guerrero et al., 2014). A number of different compounds are currently being developed (Guerrero et al., 2014; Lopez et al., 2015; Galan et al., 2016; Yin et al., 2015; Kang et al., 2015; Lee et al., 2015), but there is still more testing to do.

Recently, researchers have also started investigating rotavirus for its use in oncolytic virotherapy (Guerrero et al., 2016). Some viruses have the ability to selectively infect and kill cancer cells, a property researchers are trying to exploit to treat cancer (Huang et al., 2016; Delwar et al., 2016; Zhao et al., 2016). Rotavirus could be a good candidate for this application since it has a natural very specific cell selection mechanism (Bass et al., 1992; Fleming et al., 2011), but we need a better understanding of rotavirus infections in cancer cells to continue development of rotavirus for oncolytic virotherapy.

Mathematical models of viral infections are now being used to further our understanding of several different viruses including influenza (Baccam et al., 2006), human immunodeficiency virus (Perelson et al., 1996), hepatitis (Neumann et al., 1998), respiratory syncytial virus (Gonzalez-Parra and Dobrovolny, 2015), and ebola (Nguyen et al., 2015). These models have been used to quantify key parameters of the infection processes (Baccam et al., 2006; Perelson et al., 1996; Neumann et al., 1998; Pinilla et al.,2012), optimize drug treatment regimens (Sheikhan and Ghoreishi, 2013; Zhang et al., 2002; Padhi and Bhardhwaj, 2009; Dobrovolny et al., 2011, 2013), and understand complex host–virus interactions (Atkins et al., 2012; Dobrovolny et al., 2011, 2013; Canini and Carrat, 2011). While mathematical models have been used to study spread of rotavirus at the population level (Omondi et al., 2015; Lopman et al., 2012; Atkins et al., 2012; Pitzer et al., 2011), models of within host dynamics have not yet been applied to rotavirus.

In this paper, we use a mathematical model to extract parameters

* Corresponding author.
E-mail address: h.dobrovolny@tcu.edu (H.M. Dobrovolny).

https://doi.org/10.1016/j.virusres.2017.09.023
Received 21 November 2016; Received in revised form 5 September 2017; Accepted 28 September 2017
Available online 03 November 2017
0168-1702/

describing the in vitro viral kinetics of rotavirus for the first time. We estimate the time it takes between release of a virion and infection of the next cell, the duration of the eclipse phase. We also estimate the average number of virus particles produced by a single cell as well as the amount of virus needed to infect a cell. We then use our parameter estimates to examine how well rotavirus decreases REH cells under a variety of initial viral inocula and cell growth rate. Our findings help to quantitatively characterize rotavirus infections and represent a first step in developing rotavirus for use in oncolytic virotherapy.

2. Methods

2.1. Cells

REH cells (human acute lymphocytic leukemia non-T; non-B, ATCC1 CRL-8286™) were kindly donated by Dr. J.P. Vernot, Faculty of Medicine, Universidad Nacional de Colombia). Cell line was cultured in RPMI 1640 (Sigma–Aldrich, St. Louis, MO, USA) supplemented with 10% fetal bovine serum (FBS) (Eurobio, Les Ulis, France) and 100 μg/mL streptomycin and penicillin (Eurobio, Les Ulis, France). Cell line was cultured in a humidified atmosphere with 5% CO_2 at 37 °C. Culture was maintained by addition or replacement of fresh medium.

2.2. Wt1-5 rotavirus strain

Rotavirus Wt1-5 was isolated by Dr. C.A. Guerrero (Faculty of Medicine, Universidad Nacional de Colombia) from stool samples of five different children with diarrhea by rotavirus. Rotavirus Wt1-5 was purified as previously described in Guerrero et al. (2010, 2014). Briefly, stool samples were thawed and centrifuged at 100,000 × *g* for 90 min at 4 °C. The pellet was suspended in Tris-buffered saline (TBS) (10 mM Tris–HCl, pH 7.4, 150 mM NaCl, 1 mM $MgCl_2$, 5 mM $CaCl_2$), then mixed with one-third volume of 1,1,2-trichlorotrifluoroethane (Sigma, St. Louis, MO, USA) and emulsified by vortexing for 5 min. Phases were separated by spinning at 13,000 × *g* for 10 min at 4 °C. The aqueous phase was recovered, and the organic phase was extracted three times with TBS buffer. The combined aqueous phases were spun at 100,000 × *g* for 90 min at 4 °C, and the pellet was suspended in TBS buffer. Virus suspension was over-layered on a preformed sucrose/CsCl discontinuous gradient consisting of 1.4157 g/cm^3 (0.5 mL), 1.3039 g/cm^3 (1 mL) and 1.2070 g/cm^3 (0.5 mL) CsCl (Sigma, St. Louis, MO, USA) and an upper layer of 30% (w/v) sucrose (Sigma, St. Louis, MO, USA). Isopycnic centrifugation was performed at 280,000 × *g* for 1.5 h at 4 °C in a Sorvall TST 60.4 rotor. Visible virus bands were aspirated using a syringe and then diluted with TBS, spun at 100,000 × *g* for 1.5 h at 4 °C and the virus pellet was suspended in TBS. Rotavirus Wt1-5 was adapted to infect REH tumor cell line as previously described in Guerrero et al. (2016).

2.3. Infection of cells

To infect REH cells, Wt1-5 rotavirus was activated in serum-free medium with 1 μg/mL trypsin. Cells were washed twice in serum-free medium and then infected at two different multiplicity of infection (MOI) of 0.7 and 1.4. UV-psoralen inactivation of purified rotaviruses was performed as control as described previously (Groene and Shaw, 1992), and verified using infectivity. The inoculum was removed 1 h later and replaced with a RPMI medium containing or not 10% fetal bovine serum. This time was defined as 0 h postinfection (h.p.i.) for all experiments. Infected cells were incubated in a humidified atmosphere with 5% CO_2 at 37 °C. The percentage of rotavirus antigen-positive cells was determined every 2 h until 12 h.p.i., and a cell aliquot was also harvested at 24, 36 and 48 h.p.i. Cells were fixed with 4% paraformaldehyde (PFA) in PBS for 30 min at room temperature (RT). Afterwards, cells were washed twice with PBS and resuspended in PBS containing 0.02% sodium azide before being stored at 4 °C until use. The percentage of infected cells in terms of rotavirus antigen positive cells was assessed by immunocytochemistry.

2.4. Immunocytochemistry

Suspension cells were fixed in 4% PFA for 30 min at room temperature (RT), placed onto glass slides previously cleaned with xylol. Cells were dried for approximately 30 min in an oven at 50 °C. After permeabilization in 0.5% Triton X-100 solution for 5 min at RT, the cells were washed twice in PBS and incubated with primary rabbit polyclonal antibodies (Abs) (produced in our animal facilities) against rotavirus structural proteins (SP) for 1 h at 37 °C. After washing twice with PBS, the cells were incubated with secondary HRP-conjugated goat anti-rabbit Abs (0.133 μg/mL, Santa Cruz Biotechnology Inc., Santa Cruz, CA, USA) for 1 h at 37 °C. Following several washes with PBS, cells being positive to rotavirus antigen were visualized with 0.64 mg/mL of 3-amino-9-ethylcarbazole (AEC) substrate in 50 mM acetate buffer, pH5-0, containing 0.04% H_2O_2. Non-infected tumor cells or infected tumor cells treated with non-related antibodies were used as a control. At least ten representative images were photographically recorded using a conventional light microscope (VanGuard, Scottsdale, USA) equipped with a camera, and the mean percentage of infected cells was determined.

2.5. Cell viability test

Villus cell viability was measured using Trypan blue solution (Sigma–Aldrich, St. Louis, MO, USA) in an exclusion assay. Rotavirus-infected and mock-infected REH cells were assessed after different hours postinfection (h.p.i.). Namely, Trypan blue (0.4% in 0.81% sodium chloride and 0.06% potassium phosphate, dibasic) solution was combined with cell suspension in a 1:1 ratio, and the percentage of dead blue cells in the population quantified in a Neubauer chamber under a light microscope. As cell death control, REH cells were treated with 1 μM of H_2O_2.

2.6. Virus titration

To determine the production of infectious virions by REH tumor infected cells with the tumor cell-adapted rotavirus isolates WT1-5, the infected cells were harvested every 2 h until 12 h.p.i. Cell samples were also harvested at 24, 36 and 48 h.p.i. and it was lysed by two cycles of freezing and thawing. The supernatant from each postinfection time point was activated with trypsin and tested at serial dilutions in new REH cells. The infected cells were fixed at 12 h.p.i. as previously describe and the corresponding infectious titer was determined as focus forming units (FFU) by immunocytochemistry. Measurements were made with three replicates and the geometric mean of the three samples for each time point was used for analysis.

2.7. Gamma distributed viral kinetic model

In this paper we use a model based on an autonomous system of nonlinear ordinary differential equations to characterize the *in vitro* infection dynamics of rotavirus. The model is an extension of an infection model commonly used for influenza (Pinilla et al., 2012; Beggs and Dobrovolny, 2015; Paradis et al., 2015; Simon et al., 2016), but here we include some additional features. We include a logistic growth term $rT(1 - T/K)$ for the target cells in order to model the growth of the cells that has been observed in lab experiments. Note that death of cells is implicitly included in the growth term of the logistic model. We also include a term modeling absorption of virus into the cell, $\gamma T V$. The model is shown in Fig. 1 and is represented by the following system of equations,

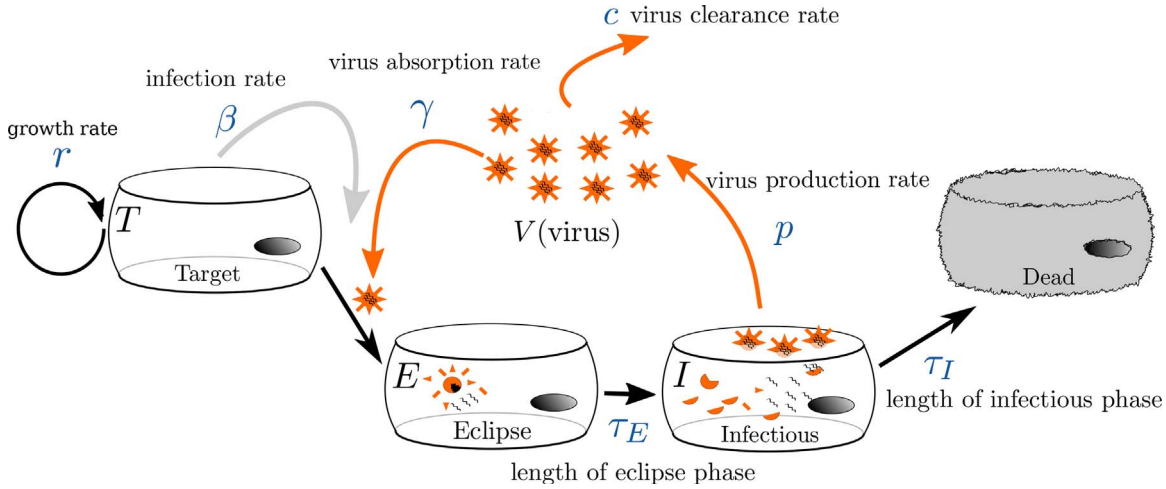

Fig. 1. Viral kinetics model. In the model, healthy target cells are infected by virus. The cells then move into an eclipse phase when the virus starts to undergo replication. The cells then transition to an infectious phase where they continuously produce virus until they die.

$$\begin{aligned}
\frac{dT}{dt} &= rT\left(1-\frac{T}{K}\right)-\beta T V\\
\frac{dE_1}{dt} &= \beta T V-\frac{n_E}{\tau_E}E_1\\
\frac{dE_j}{dt} &= \frac{n_E}{\tau_E}E_{(j-1)}-\frac{n_E}{\tau_E}E_j \quad \text{for } j=(2,\ldots,n_E)\\
\frac{dI_1}{dt} &= \frac{n_E}{\tau_E}E_{n_E}-\frac{n_I}{\tau_I}I_1\\
\frac{dI_j}{dt} &= \frac{n_I}{\tau_I}I_{(j-1)}-\frac{n_I}{\tau_I}I_j \quad \text{for } j=(2,\ldots,n_I)\\
\frac{dV}{dt} &= p\sum_{j=1}^{n_I}I_j-cV-\gamma T V.
\end{aligned} \tag{1}$$

In this model, uninfected target cells, T, are infected at a rate β when they encounter a virion V. Target cells reproduce according to a logistic model, where the growth rate r decreases as the number of cells approaches a maximum carrying capacity of K. The newly infected cells, E, first enter the eclipse phase, where the cells are infected but not yet actively producing virions. After an average time τ_E, the cells transition to the infectious phase, I, where they actively produce virus at a rate p. After an average time τ_I, infectious cells die. Virus is cleared, through loss of infectivity, from the system at a rate c, and is absorbed into target cells at a rate γ. The transitions between eclipse/infectious cells and infectious/dead cells are modeled as gamma distributions, which are more biologically realistic than the exponential transitions, which assume that cells can immediately begin viral production upon infection, and can produce virus indefinitely, used in more basic viral infection models (Holder and Beauchemin, 2011). n_E and n_I are the number of compartments used to represent the eclipse phase and infectious phase, respectively. In the gamma distributed model the standard deviations of the eclipse and infectious phases are $\sigma_E=\tau_E/\sqrt{n_E}$ and $\sigma_I=\tau_I/\sqrt{n_I}$.

2.8. Fitting algorithms

We determine the best fit by minimizing the sum of squared residuals (SSR) between the experimental and predicted values, although we use a modified sum of squared residuals function to deal with the different types of data in this experiment. We include four terms related to viral load and infected cells for the two different MOIs (0.7 and 1.4). This type of approach has been used before in viral dynamics (Cao et al., in press; Pawelek et al., 2012). In this case the SSR has four parts, one for each for the viral titer and infected cells for both of the MOIs. For each of these components, the SSR is calculated with,

$$\text{SSR}=\sum_{i=1}^{n}(\log(y_i)-\log(f(t_i)))^2, \tag{2}$$

where n is the number of experimental data points, $\log(y_i)$ are the logarithmic values of the experimental data points, $\log(f(t_i))$ are the model predictions (either virus or infected cells). All data points are weighted equally. A small SSR indicates a tight fit of the model to the experimental data. In order to ensure that parameter estimates are biologically realistic, we placed bounds on some of the parameters (Table 1).

Fitting was done in two stages. We first fit the growth kinetics of REH cells using the logistic model in order to extract the growth rate r and maximum number of cells K. The values of these two parameters were then fixed as we fit the viral kinetics model (Eq. (1)) to experimental data. To extract viral kinetics parameters, we simultaneously fit both the low MOI (0.7) and high MOI (1.4) experiments. We assumed that the viral kinetics parameters are the same for both experiments, but that the initial conditions differ. In the experiments, virus is added to the cells for one hour and then washed away. To best replicate these conditions, we assume that the infections are initiated with cells in the eclipse phase. The amount of virus initially added to the cell culture is $V(0)=\text{MOI}*T(0)$. In one hour, this amount of virus will infect $\beta*T(0)*V(0)\Delta t$ ($\Delta t=1$ h) cells. We assume that when the virus is washed away, the infected cells will still be in the eclipse phase, so our infection is initiated with $E_1(0)=\beta*T(0)^2*\text{MOI}$ cells in the first compartment of the eclipse phase. We fix the initial number of target cells to the experimentally measured initial value of $T(0)=1.58\times10^6$ cells. All other compartments of the eclipse phase, all compartments of the infectious phase and virus are assumed to be zero initially.

We used two algorithms to find the minimum SSR. We initially used a genetic algorithm (Golberg, 1989) which performs a very broad search of the parameter space and is less dependent on the initial guess. This algorithm is based on a natural selection process that mimics biological evolution. The algorithm changes a population of individual solutions such that at each step, the algorithm randomly selects solutions from the current population and uses them as seeds to produce the parameter estimates for the next generation. Over many iterations, the

Table 1
Parameter bounds used for fitting.

Parameter	Meaning	Bounds
p	Viral production rate	10^0–10^{10} FFU/mL cell^{-1} h^{-1}
β	Infection rate	10^{-10}–1 (FFU/mL)$^{-1}$ h^{-1}
c	Viral clearance rate	10^{-4}–10^1/h
τ_I	Mean duration of infectious phase	0.25–120 h
τ_E	Mean duration of eclipse phase	0.25–120 h
n_I	Number of stages of infectious phase	1–100
n_E	Number of stages of eclipse phase	1–100

population "evolves" toward an optimal solution (Golberg, 1989; Holland, 1992; Conn et al., 1997). There are many parameters that can be varied in the genetic algorithm. We used different scenarios for parameters such as population size, the number of generations, and the initial population function, among others. Due to the random nature of the genetic algorithm a range of solutions are obtained, which helps to cover the large search space. It is important to remark that the genetic algorithm is well suited to find global optimums instead of local ones. We ran the global optimization algorithm 1000 times with different scenarios (initial guess, parameters of the optimization process) in order to improve the probability of finding the global optimum parameter set.

Once the genetic algorithm found a good fit, these parameters were used as the initial guess for the trust-region-reflective and interior point algorithms (Coleman and Li, 1996; Press et al., 1992), which search a more localized region of the parameter space. The use of several different algorithms increases the probability of finding the global minimum for the SSR, which is not a straightforward task for this model. All fitting was implemented in Matlab using the `ga` and the `fmincon` functions of the `optimization` package.

To estimate the error in our parameter estimates, we compute the 95% confidence intervals for each of the parameters using bootstrapping. Specifically, we use the percentile bootstrap method, i.e., using percentiles of the bootstrap distribution (Davison and Hinkley, 1997; Efron, 1979). Fit residuals were sampled with replacement to produce 1000 bootstrap replicates of the data sets and used to estimate the 95% confidence intervals. In addition, we used the profile likelihood method which is a generalization of classical approaches like standard errors which are based on the Fisher-Information matrix. The profile likelihood provides reasonable confidence intervals for parameter estimation of ODE models and allows assessment of the identifiability of model parameters (Kreutz et al., 2012; Raue et al., 2009, 2013; Tönsing et al., 2017; Raue et al., 2013).

3. Results

3.1. Growth dynamics of REH cells

As described in the methods, we first fit a logistic growth model to experimental data capturing growth of REH cells. The experimental data and the best model fit along with best fit parameter values are shown in Fig. 2. The growth rate, r, is related to doubling time (DT) through $\mathrm{DT} = \frac{\ln(2)}{r}$, so we find that the doubling time of these cells is 6.8 h. This is faster than previous estimates of 21 and 26 h (Atzpodien et al., 1986; Aldridge and Radford, 1998), although these previous estimates assumed exponential growth so their estimates might be slower to correct for saturation effects.

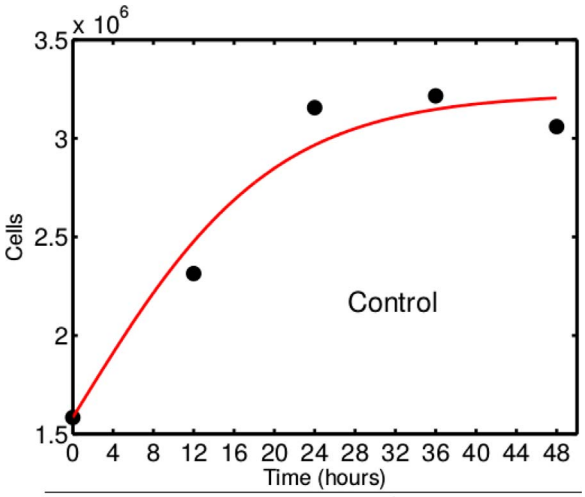

Parameter	Value
r (/h)	0.103 (0.0800–0.132)
K (cells)	3.23×10^6 $(3.07–3.42)\times10^6$
SSR	1.47×10^{11} $(0.518–5.18)\times10^{11}$

Fig. 2. Best fit of the logistic growth model to experimental growth of REH cells. Black circles give the experimental data and the red line shows the best model fit. Best fit parameter values and 95% confidence intervals are given in the table.

3.2. Parameter estimates for rotavirus dynamics in the REH cell line

Having determined the parameters describing growth dynamics of REH cells, we fixed those parameters and fit the viral time course and infected cell data with the viral kinetics model, Eq. (1). Fig. 3 shows the experimental data for both the 0.7 MOI (left) and 1.4 MOI (right) experiments and the best fit model dynamics. The model (1) is able to reproduce the kinetics of both the rotavirus and the infected cells. Best fit parameters along with 95% confidence intervals using the percentile bootstrap method are given in Table 2.

In addition to the parameters used directly in the model, Table 2 presents parameter combinations that provide biologically interesting quantities. Note that while our fitting algorithm has returned a possible set of parameters, they might not be the only parameter set that adequately explains the data. We found that the duration of the eclipse phase, which is the time between viral entry and production of the first virion, is 7.25 h. This means that it takes, on average, about 7 h for synthesis of viral proteins, replication, and assembly of the virus. We also found that the duration of the infectious phase, which is the time period when cells are actively producing virus is 46.2 h. Together, these quantities tell us that cells infected with rotavirus will live, on average, for ~53 h after they are infected, with the majority of that time spent actively producing virus. We can also derive the standard deviations for the durations of the eclipse and infectious phases (σ_E and σ_I). For a gamma-distributed process, the standard deviation is $\sigma = \tau/\sqrt{n}$. For rotavirus, the standard deviations are 16.3 h for the infectious phase and 2.29 h for the duration of the eclipse phase. These distributions are pictured in Fig. 4 where we plot the probability of a cell transitioning out of a particular phase as a function of the time it has spent in that phase.

Another time duration of interest is the infecting time, t_{inf}, defined as the average time it takes for an infectious cell to infect another cell (Holder and Beauchemin, 2011), and given by $t_{\mathrm{inf}} = \sqrt{2/\beta p T_0}$. We found that this process was very fast for rotavirus, only taking about 2 min.

Finally, we calculate some quantities that quantify virus-cell interactions. The quantity γ/β gives the amount of virus that is absorbed into a cell in order for it to become infected. We found that for rotavirus 1410 FFU/mL cells^{-1} is absorbed before a cell becomes infected. While this might seem like a large number, it is not clear how many infectious virions are in 1 FFU/mL (Heider and Metzner, 2014). Once infected, $p\tau_I$ gives the average amount of virus produced over the infectious lifetime of a single cell, which we found to be 1.42×10^5 FFU/mL cells^{-1}. The basic reproductive number, R_0, given by

$$R_0 = \frac{\beta p \tau_I T_0}{c + \gamma T_0} \tag{3}$$

for this model (Beauchemin et al., 2008), represents the average number of secondary infections caused by a single infected cell introduced into a susceptible population. Our calculated value of $R_0 = 100$ is in line with our estimates that 1.42×10^5 FFU/mL cells^{-1} are produced by an infectious cell, but that 1410 FFU/mL cells^{-1} are needed to infect a second cell. This also suggests, then, that viral clearance is negligible over the time span that it takes to infect a cell. Note that while there might be some uncertainty in the parameter estimates from our choice of T_0 and V_0, changing the initial number of target cells will rescale the production rate only, while changing the

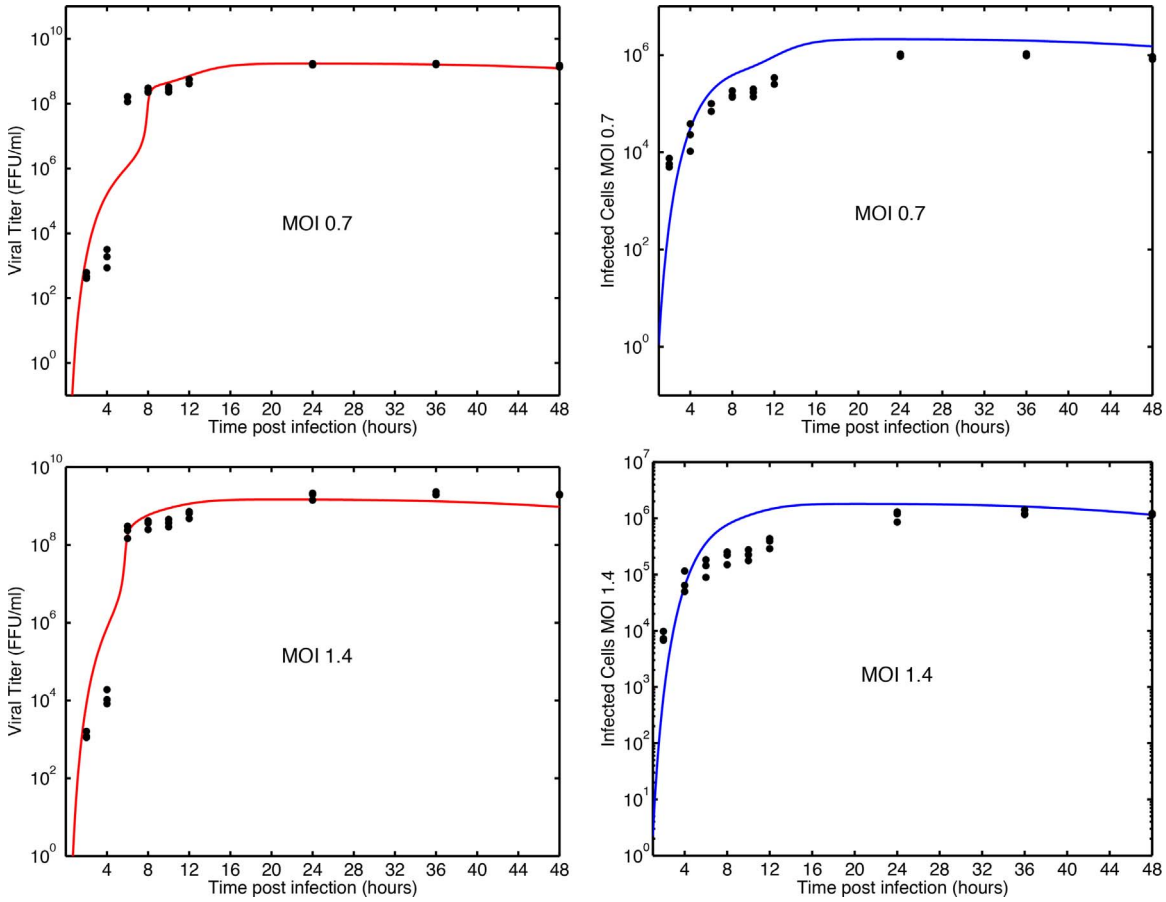

Fig. 3. Best fit of the viral kinetics model to rotavirus infection of REH cells. Black circles indicate experimental data and lines represent the best model fit. Viral titer (left column) and infected cells (right column) are shown for infections with an MOI of 0.7 (top row) and an MOI of 1.4 (bottom row).

Table 2
Estimated parameters for rotavirus *in vitro* infection in tumor cell lines.

Parameter	Value	95% confidence interval from bootstrapping	95% confidence interval from likelihood profile
β (FFU/mL^{-1} h^{-1})	3.24×10^{-7}	$(2.94–3.66) \times 10^{-7}$	$(2.95–4.25) \times 10^{-7}$
p (FFU/mL cells^{-1} h^{-1})	3070	2740–3740	2340–5150
c (/h)	3.77	3.17–3.97	1.32–11.0
τ_I (h)	46.2	44.1–50.3	28.5–∞
τ_E (h)	7.25	6.42–7.74	6.39–7.83
n_I	8	—	—
n_E	10	—	8–13
γ (cells^{-1} h^{-1})	4.57×10^{-4}	$(4.16–4.85) \times 10^{-4}$	$(1.57–6.57) \times 10^{-4}$
SSR	18.3	16.7–19.0	
σ_I (h)	16.3	15.6–17.8	
σ_E (h)	2.29	2.14–2.58	
t_{inf} (h)	0.0350	0.0314–0.0372	
γ/β (FFU/mL cells^{-1})	1410	1210–1550	
$p\tau_I$ (FFU/mL cells^{-1})	1.42×10^{5}	$(1.25–1.87) \times 10^{5}$	
R_0	100	88.5–160	

initial viral load will rescale the infection rate and the production rate. In either case, R_0 and infecting time t_{inf} are not affected by rescaling since they involve combinations of parameters. Also, any parameter that has units of time only (clearance rate, duration of eclipse and infectious phases) is also not affected by rescaling of target cells or virus.

We used a variety of methods to assess the goodness of fit of the model to the experimental data. First, we examined the likelihood profiles which are an excellent tool to check that we have reached at least a local minimum and have structural identifiability of the parameters (Kreutz et al., 2012; Raue et al., 2009). These are shown in Fig. 5 with 95% significance thresholds indicated by dashed lines. Almost all parameters are well-identified since they lie at the minimum of the SSR function, with the exception of n_I and τ_I. For n_I, several different values give equal SSRs, so it is not identifiable. Previous work fitting a similar model to influenza viral loads found the same issue and researchers in that case decided to fix n_I, in order to avoid this identifiability issue (Pinilla et al., 2012; Paradis et al., 2015; Simon et al., 2016). The profile likelihood reveals that the parameter τ_I is practically non-identifiable for increasing parameter values despite achieving a minimum value of SSR. Since the likelihood profile does not cross the significance

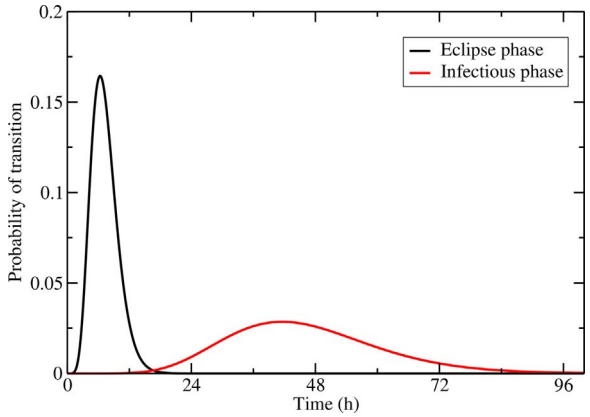

Fig. 4. Probability distribution functions of the eclipse and infectious durations of rotavirus. The curves indicate the probability of transitioning out of the eclipse state (black line) or the infectious state (red line) as a function of the time spent in that state. (For interpretation of the references to color in this figure legend, the reader is referred to the web version of this article.)

threshold on one side, there is no upper bound to the acceptable values of τ_I (Raue et al., 2009). In addition to the profile likelihood we present in Table 2 the simultaneous confidence intervals to a confidence level of 95%. These likelihood-based confidence intervals are considered superior to asymptotic confidence intervals for finite samples (Raue et al., 2009). While the likelihood profiles suggest that we have reached a local minimum, it is not necessarily the global optimum.

As a measure of the variability in our parameters, we include the five best fit values found using the genetic algorithm in Table 3. Based on these results we can infer that that the model is not globally identifiable, as different sets of parameters can produce similar SSRs. The best results are relatively consistent at least in the order of magnitude of the parameter values. Due to the number of free parameters, it is not unexpected that we will find many local optima when searching for a global one. The best five fits presented here give us another measure of the possible uncertainty in our estimates. For example, t_{inf} values vary between 1.22 and 2.46 min, which is a reasonable range. For R_0, we obtain a range from 100 to 301, which seems quite large. However, the interesting value of R_0 is 1 since that marks the boundary between growth and suppression of an infection. Previous work has suggested that once $R_0 > 7$, the value of R_0 is not indicative of any change in dynamics (Smith et al., 2010). While a change in R_0 from 100 to 300 seems large, the change in infection dynamics given these values of R_0 is very small.

Another method for assessing the identifiability of parameters is to look for correlations in parameter estimates. We do this by creating scatter plots of pairs of parameters from our bootstrap results, as shown in Fig. 6. We see no correlations between any of the parameter estimates. Finally, we also performed a sensitivity analysis using the best fit parameters given in Table 2. We increased and decreased the parameter values by different percentages (from 50% to 400%) based on the variability of each parameter in Table 3 to see their effects on rotavirus dynamics. As can be seen in Fig. 7 the plots show the robustness of the outcomes of the model respect to changes on the parameter values. Both the viral time courses and the infected cell time courses seem to be most sensitive to changes in τ_E, particularly in the early stages of the infection. The infection rate, production rate, and clearance rate all

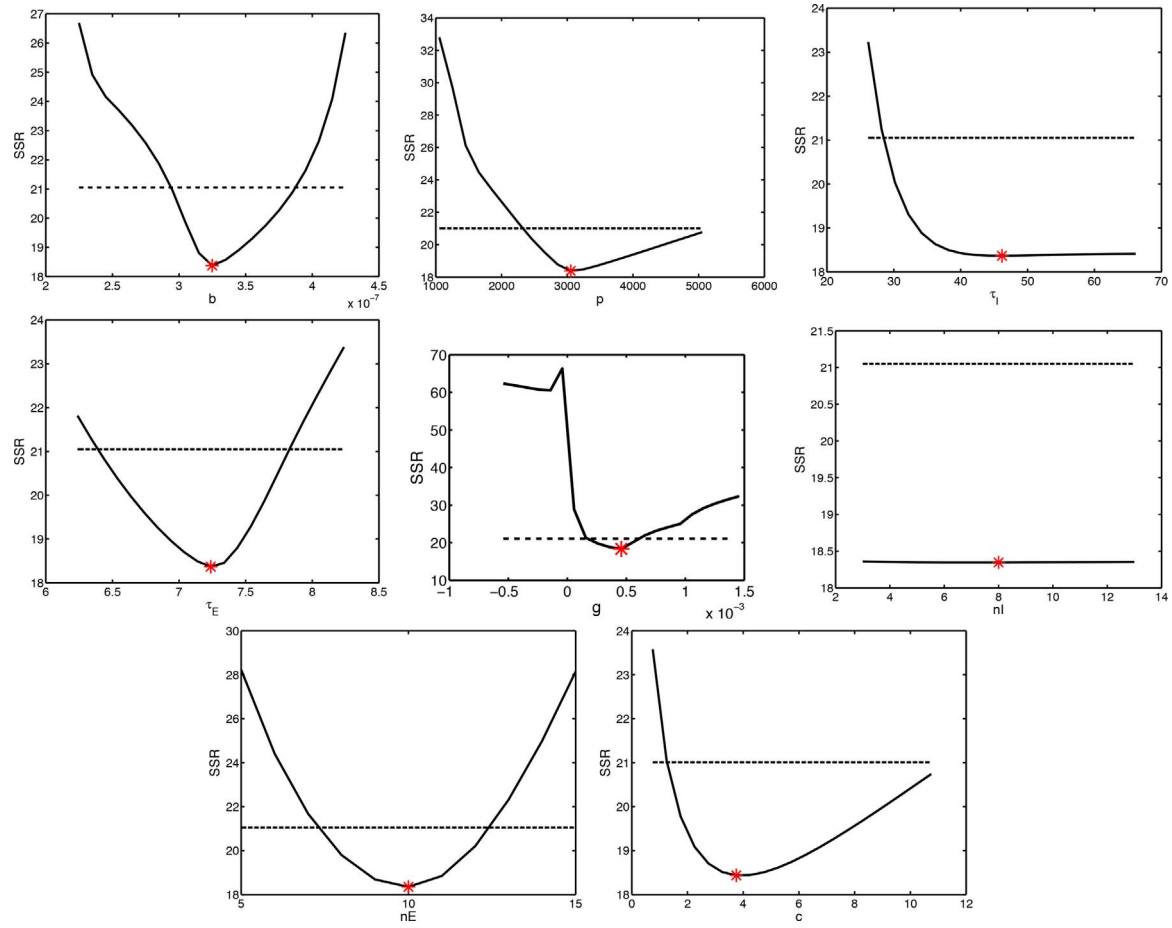

Fig. 5. Likelihood profiles of the fit to the rotavirus data. Profiles show the change in SSR as each parameter is varied from its best fit value. Dashed lines indicate the 95% significance level.

Table 3
Best sets of the estimated parameters for rotavirus *in vitro* infection in tumor cell lines.

β (FFU/mL^{-1} h^{-1})	p (FFU/mL cells^{-1} h^{-1})	c (/h)	τ_I (h)	τ_E (h)	n_I	n_E	γ (cells^{-1} h^{-1})	SSR
3.24×10^{-7}	3070	3.77	46.2	7.2	8	10	4.57×10^{-4}	18.34
3.09×10^{-7}	7710	11.2	51.4	6.9	7	11	1.12×10^{-3}	18.34
3.26×10^{-7}	9370	10.0	53.4	10.3	3	7	5.35×10^{-4}	18.39
2.68×10^{-7}	6380	8.39	50.4	6.8	7	11	6.31×10^{-4}	18.43
3.34×10^{-7}	2250	2.22	50.3	9.8	2	7	1.58×10^{-4}	18.54

affect the viral time course, but do not change the time course of infected cells. The confidence interval estimates for each parameter, the likelihood profiles, correlation analysis and the sensitivity analysis give a measure of the variability of each of the parameters. Based on these results, we can suggest that rotavirus dynamics can be modeled reasonably well by the proposed mathematical model with the parameter values presented.

3.3. Viral suppression of REH cell growth

One advantage of a mathematical model is that we can predict the time course of components of the system that are not measured, or we can predict the time course at time points that have not been measured experimentally. In Fig. 8, we show the time courses of target, eclipse, and infectious cells, as well as the viral titer for the two experiments presented earlier. We see that for both MOIs, the target cells (red lines) are depleted very quickly; in less than 12 h after initiation of the infection, all the REH cells have been infected. While the cells are infected quickly, they take a longer time to be cleared. While the cells pass through the eclipse phase (green lines) fairly quickly (about 24 h after initiation of infection), infectious cells (blue lines) persist for as long as seven days after initiation of infection. Since infectious cells are still producing virus, this means that the viral titer will also remain high while there are still infectious cells remaining.

Not only can we extend the results of specific experiments, in order to better understand how each variable changes over the course of the infection, but we can also use the mathematical model to examine the effect of different variables. There are two reasons to use models in this way, the first is to make predictions that can be tested experimentally to further validate (or reject) the model. The second reason is to understand the role of variables that are difficult to manipulate experimentally. One reason we are interested in examining the viral kinetics of rotavirus is because it is being investigated for oncolytic therapy (Guerrero et al., 2016), so an endpoint of interest is the length of time it takes to kill all the cancer cells. In Fig. 9, we examine how long it takes to eradicate all REH cells in the assay as a function of MOI (left) or cell growth rate (right). We see that as MOI decreases, the time to eradicate the cells increases. This is because the early cycles of infection infect only a few cells when MOI is small. At high MOI, the time to eradicate the cells becomes constant. This time of $\sim$179 h represents the minimum time required for all cells to become infected and move through both the eclipse and infectious phases. The cell growth rate does not affect the time to cell eradication quite as much as changes in the MOI. There is a slight increase in the time to cell eradication as the

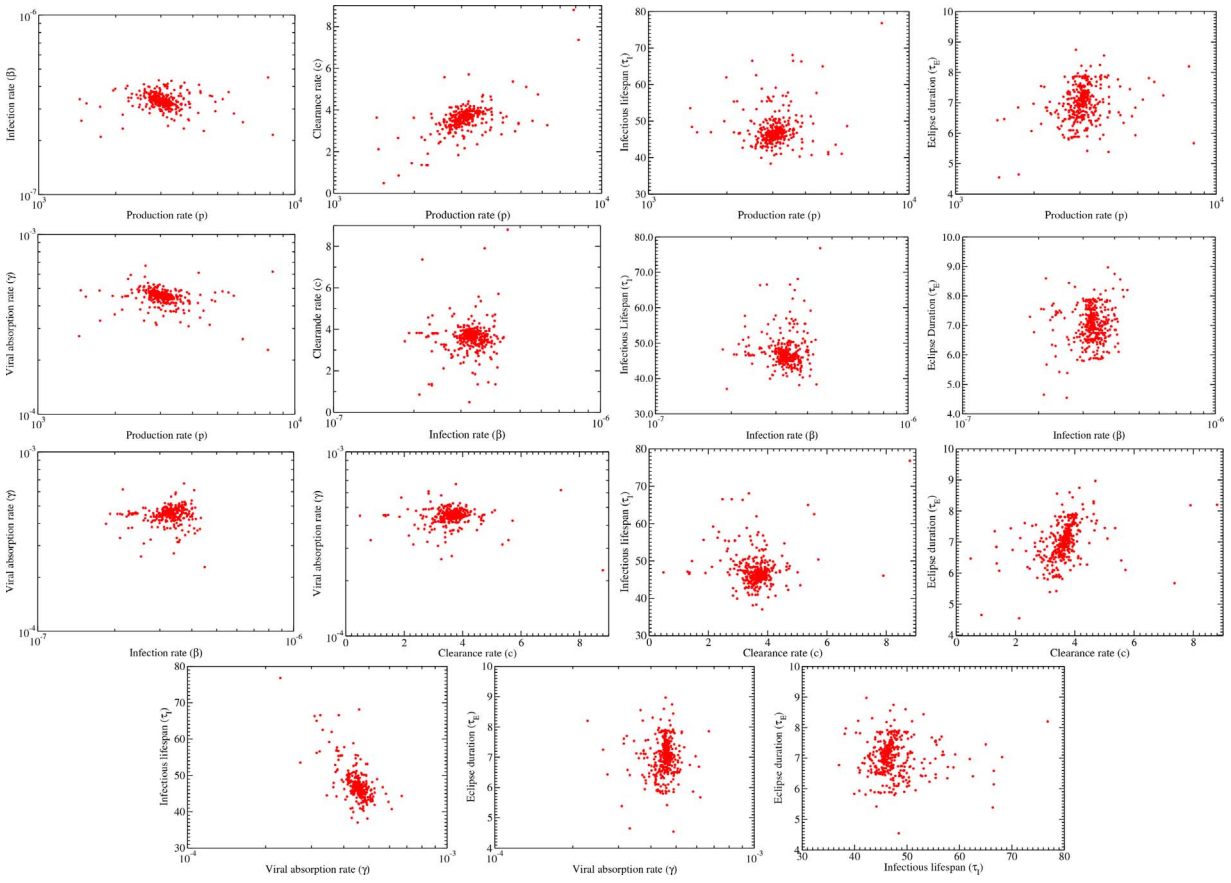

Fig. 6. Bootstrapping results using the best parameters given in Table 2.

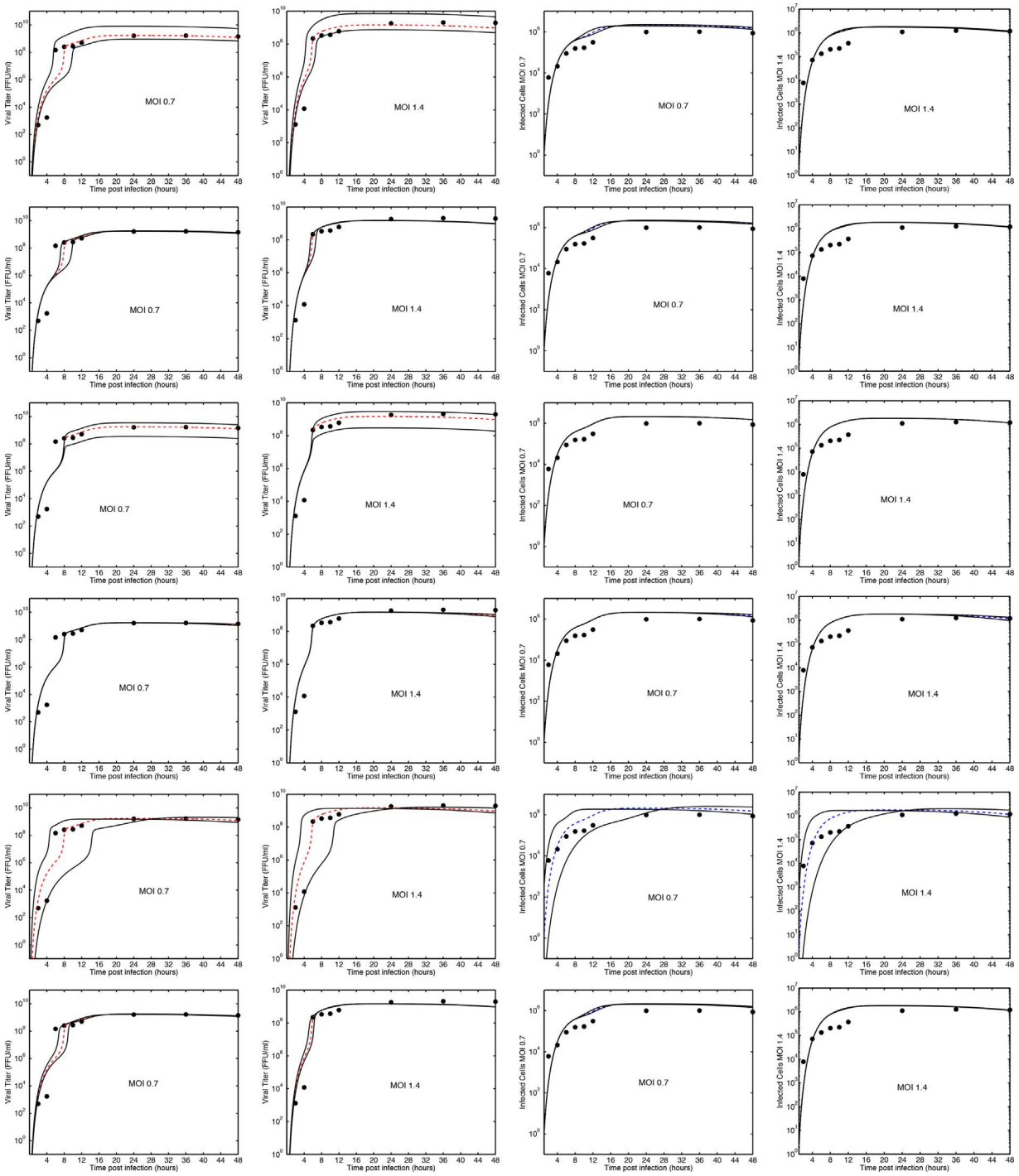

Fig. 7. Sensitivity analysis using the best parameters given in Table 2. The parameter values have been increased and decreased by 50–400% to see their effects on rotavirus dynamics. Each column shows a quantity measured: virus MOI 0.7 (left column), virus MOI 1.4 (1st center column), infected cells MOI 0.7 (2nd center column), and infected cells MOI 1.4 (right column). Each row shows the results for a particular parameter: virion production rate p (first row), β (second row), clearance rate c (third row), infected phase τ_I (fourth row), eclipse phase τ_E (fifth row) and binding rate g (last row).

growth rate increases, an effect that is more apparent at low MOI.

4. Discussion and conclusions

This paper presented the first fits of a viral kinetics model to an *in vitro* rotavirus infection. While not all of the parameters estimated here are identifiable, it is interesting to compare our estimates to previous work in an effort to assess their accuracy. Unfortunately, since *in vitro* rotavirus dynamics have not yet been quantified in this way, it is difficult to perform this kind of comparison for all the estimated parameters. Some previous studies measured the duration of the eclipse phase more directly, finding that the duration of the eclipse phase for ovine rotavirus is 6 h (Berrios et al., 1993) and for rhesus rotavirus is 8 h (Bass et al., 1992), both of which are fairly close to our estimate of 7.25 h. In another study, Makabe et al. (1986) noted that there was evidence of cell death at about 2 days post infection for ovine rotavirus, consistent with our estimates of the distribution of cell lifespans. Bass et al. (1992) also measured the average amount of virus produced per infected cell for four cell lines, finding that infected cells produced between 49–146 pfu/cell. Our estimate is much larger than this, but

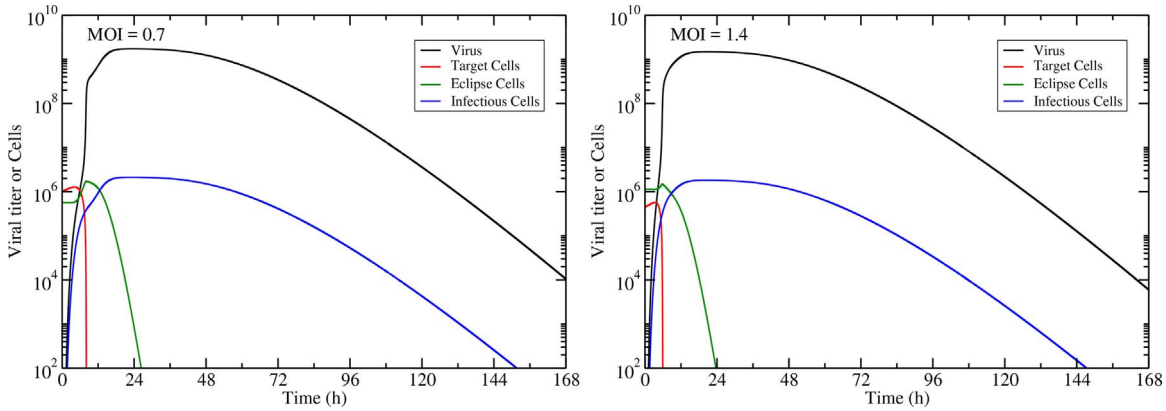

Fig. 8. Model predictions of the time course of the infection. We show the full time courses for all elements of the MOI = 0.7 experiment (left) and MOI = 1.4 experiment (right). Viral titer is indicated by the black line, target cells are given by the red line, eclipse cells are given by the green line, and infectious cells are given by the blue line. (For interpretation of the references to color in this figure legend, the reader is referred to the web version of this article.)

infectious virus in our experiment is measured using a different technique, so the two values cannot be properly compared (Kitamoto et al., 1991).

A particularly interesting parameter estimate is the very rapid infecting time of 2 min. In these 2 min, the newly-formed virion leaves one cell and migrates to another, which seems to be a rather short time for a particle to diffuse to a new location and gain entry into the cell. However, some studies have determined that rotavirus can gain entry into a cell in less than 5 min (Suzuki et al., 1985; Kaljot et al., 1988). There is also some evidence that under certain conditions, rotavirus can cause fusion of cell membranes (Knipping et al., 2012; Falconer et al., 1995; Gilbert and Greenberg, 1997; Gelberg et al., 1990), thus spreading directly from cell to cell rather than through extracellular diffusion, a much faster transmission process. While seemingly short, given this experimental evidence, our estimate of the infecting time might not be unreasonable.

Once parameterized, we used our model to examine whether rotavirus is a good candidate for use in oncolytic virotherapy. Specifically, we assessed how quickly rotavirus cleared all the REH cells in our system. We found that there was a strong dependence of cancer cell eradication time on the initial viral inoculum (MOI), but there is little sensitivity of cell eradication time on cell growth rate. The predicted model dependency of cell eradication time on MOI is a feature of the model that can be tested experimentally to provide further support or perhaps to reject the model. The model prediction of cell eradication time dependence on growth rate is difficult to test experimentally, but has some important implications for possible use of rotavirus in oncolytic therapy. Since tumor growth rate is known to vary from patient to patient (Nayyar et al., 2016), the fact that rotavirus seems to effectively suppress cells with different growth rates means it should be broadly effective in vivo. We must be careful about introducing the correct initial viral inoculum, however, since low MOI leads to longer suppression times. The average number of tumor cells in a patient is much higher than the number of cells in our system, so it is unlikely that high MOIs will be used to treat patients, so careful consideration of the dose will be needed.

A particular concern when using this type of analysis is that we have found the global minimum for the SSR and that the model parameters are identifiable. However, in many cases it is difficult to prove or achieve either of these (Chis et al., 2011; Nguyen et al., 2016). For example, in Wu et al. (2008), the authors did an algebraic identifiability analysis for a similar, but simpler, model of only three ordinary differential equations. Our gamma model has a variable number of ordinary differential equations but roughly more than twenty, so the mathematics needed for analysis of this model are even more complex. Structural identifiability analysis cannot simply be scaled-up from a three equation model to a model with a larger number of equations. It is important to be aware that despite the interest in knowing a priori whether there is any chance of uniquely estimating all model unknown parameters, the structural identifiability analysis for general non-linear dynamic models is still an open question (Chis et al., 2011; Nguyen et al., 2016). While it is not the same as doing a full mathematical analysis of the identifiability of our model, we can use the work of others to infer the identifiability of our parameters. In Pinilla et al. (2012), the authors did an identifiability analysis of a similar gamma-distributed model and found that the only parameter not identifiable was the standard deviation of the infectious life span which is related to the number of stages of the infectious phase n_I. In our case, we have

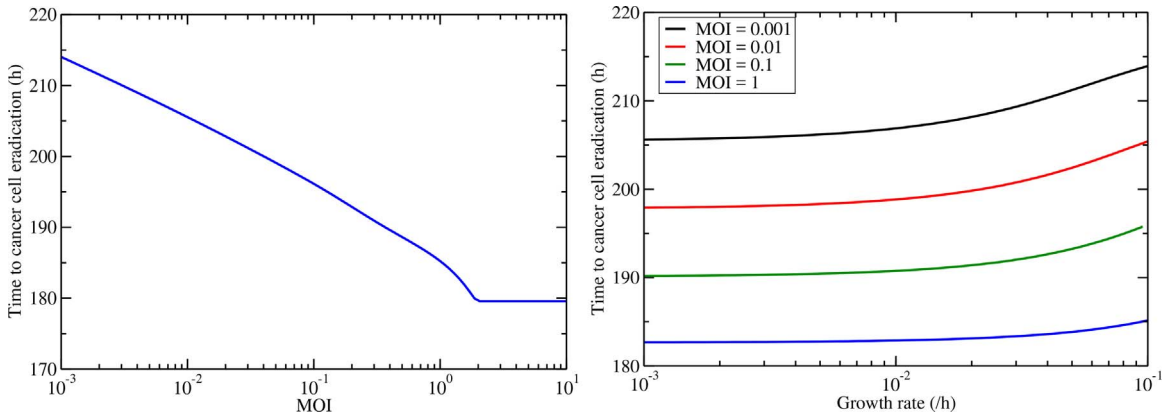

Fig. 9. Time to eradication of all REH cells in the experimental system as a function of MOI (left) or cell growth rate (right).

some additional data regarding the infected cells which provides extra information available for the fitting process. Specifically, having the time course of infected cells as well as the time course of virus allows for differentiation of virus and infected cell lifetimes which cannot be separately identified from viral time course alone (Smith et al., 2010). Unfortunately, even this extra data did not result in practical identifiability of n_I and τ_I in this case. Full experimental validation of the model would require further experiments at different MOIs with data collected over a longer period of time.

The methodology presented here, fitting mathematical models to experimental data, allows us to quantify different aspects of the viral life cycle. While this information is helpful for developing our understanding of rotavirus replication, it also has other applications. This technique can be used to quantitatively compare two different viral strains to better assess fitness or virulence (Pinilla et al., 2012; Paradis et al., 2015; Simon et al., 2016). It can also be used to infer the mechanism of action of antivirals by quantifying changes in different parts of the viral replication cycle when antivirals are used (Beauchemin et al., 2008; Gonzalez-Parra et al., 2016). In the case of rotavirus, it could be used to quantitatively compare growth of rotavirus in different tumor cell lines as part of the assessment of its potential use in oncolytic virotherapy.

While our model captures the basic features of rotavirus infection, there are some biological processes that have been neglected in the current study that will need to be considered in future work. As noted earlier, there is some evidence that rotavirus can cause cell membrane fusion and transmit directly from one cell to another (Knipping et al., 2012; Falconer et al., 1995; Gilbert and Greenberg, 1997). This mode of transmission is not explicitly described in our model, although its effect is seen in the short infecting time. Our model also does not include the immune response to rotavirus. Studies have shown that rotavirus triggers a rapid innate immune response (Holloway and Coulson, 2013), but that rotavirus has developed mechanisms to evade this response (Arnold, 2016; Morelli et al., 2015). These types of complex interactions would require several extra parameters and without additional experimental data, the immune parameters cannot be accurately estimated. Thus, further studies are necessary in order to develop more complex models and better characterize rotavirus replication.

Acknowledgements

The authors are grateful to the anonymous reviewers of this journal for providing us with insightful comments that helped us improve the clarity and the quality of the paper. This research was supported by Colciencias grant 110171250829 from the National System of Science, Technology and Innovation from Colombia.

References

Aldridge, D.R., Radford, I.R., 1998. Explaining differences in sensitivity to killing by ionizing radiation between human lymphoid cell lines. Cancer Res. 58, 2817–2824.
Arnold, M., 2016. The rotavirus interferon antagonist NSP1: many targets, many questions. J. Virol. 90 (11), 5212–5215. http://dx.doi.org/10.1128/JVI.03068-15.
Atkins, K.E., Shim, E., Pitzer, V.E., Galvani, A.P., 2012. Impact of rotavirus vaccination on epidemiological dynamics in England and Wales. Vaccine 30 (3), 552–564.
Atzpodien, J., Gulati, S.C., Clarkson, B.D., 1986. Comparison of the cytotoxic effects of merocyanine-540 on leukemic cells and normal human bone marrow. Cancer Res. 46, 4892–4895.
Baccam, P., Beauchemin, C., Macken, C.A., Hayden, F.G., Perelson, A.S., 2006. Kinetics of influenza A virus infection in humans. J. Virol. 80 (15), 7590–7599. http://dx.doi.org/10.1128/JVI.01623-05.
Bass, D., Baylor, M., Chen, C., Mackow, E., Bremont, M., Greenberg, H., 1992. Liposome-mediated transfection of intact viral particles reveals that plasma membrane penetration determines permissivity of tissue culture cells to rotavirus. J. Clin. Invest. 90 (6), 2313–2320. http://dx.doi.org/10.1172/JCI116119.
Beauchemin, C.A., McSharry, J.J., Drusano, G.L., Nguyen, J.T., Went, G.T., Ribeiro, R.M., Perelson, A.S., 2008. Modeling amantadine treatment of influenza A virus in vitro. J. Theor. Biol. 254, 439–451. http://dx.doi.org/10.1016/j.jtbi.2008.05.031.
Beggs, N.F., Dobrovolny, H.M., 2015. Determining drug efficacy parameters for mathematical models of influenza. J. Biol. Dyn. 9 (S1), 332–346. http://dx.doi.org/10.1080/17513758.2015.1052764.
Bennett, A., Bar-Zeev, N., Cunliffe, N.A., 2016. Measuring indirect effects of rotavirus vaccine in low income countries. Vaccine 34 (37), 4351–4353. http://dx.doi.org/10.1016/j.vaccine.2016.07.001.
Berrios, P., Celedon, M., Alvarado, M., Santibanez, M., 1993. Ovine rotavirus – characterization of the strain Leyda-1987. Arch. Med. Vet. 25 (2), 199–205.
Black, R.E., Cousens, S., Johnson, H.L., Lawn, J.E., Rudan, I., Bassani, D.G., Jha, P., Campbell, H., Walker, C.F., Cibulskis, R., et al., 2010. Global, regional, and national causes of child mortality in 2008: a systematic analysis. Lancet 375 (9730), 1969–1987.
Bruun, T., Salamanca, B.V., Bekkevold, T., Vainio, K., Gibory, M., Haugstad, K.E., Rojahn, A., Jakobsen, K., Storvold, G., Lunde, A., Stordal, K., Kanestrom, A., Eidem, M.O., Dollner, H., Skanke, L.H., Nordbo, S.A., Sivertsen, H.C., Gilje, A.M., Haarr, E., Flem, E., 2016. Burden of rotavirus disease in norway using national registries for public health research. Ped. Infect. Dis. J. 35 (4), 396–400. http://dx.doi.org/10.1097/INF.0000000000001055.
Canini, L., Carrat, F., 2011. Population modeling of influenza A/H1N1 virus kinetics and symptom dynamics. J. Virol. 85 (6), 2764–2770. http://dx.doi.org/10.1128/JVI.01318-10.
Cao, P., Wang, Z., Yan, A.W., McVernon, J., Xu, J., Heffernan, J.M., Kedzierska, K., McCaw, J.M., 2016;al., in press. On the role of cd8+ t cells in determining recovery time from influenza virus infection. Front. Immunol. 7.
Chis, O.-T., Banga, J.R., Balsa-Canto, E., 2011. Structural identifiability of systems biology models: a critical comparison of methods. PLoS ONE 6 (11), e27755.
Coleman, T.F., Li, Y., 1996. An interior trust region approach for nonlinear minimization subject to bounds. SIAM J. Optim. 6 (2), 418–445.
Conn, A., Gould, N., Toint, P., 1997. A globally convergent lagrangian barrier algorithm for optimization with general inequality constraints and simple bounds. Math. Comput. Am. Math. Soc. 66 (217), 261–288.
Davison, A.C., Hinkley, D.V., 1997. Bootstrap Methods and Their Application, vol. 1 Cambridge University Press.
Delwar, Z., Zhang, K., Rennie, P.S., Jia, W., 2016. Oncolytic virotherapy for urological cancers. Nat. Rev. Urol. 13 (6), 334–352. http://dx.doi.org/10.1038/nrurol.2016.84.
Dobrovolny, H.M., Gieschke, R., Davies, B.E., Jumbe, N.L., Beauchemin, C.A.A., 2011. Neuraminidase inhibitors for treatment of human and avian strain influenza: a comparative study. J. Theor. Biol. 269 (1), 234–244. http://dx.doi.org/10.1016/j.jtbi.2010.10.017.
Dobrovolny, H.M., Reddy, M.B., Kamal, M.A., Rayner, C.R., Beauchemin, C.A., 2013. Assessing mathematical models of influenza infections using features of the immune response. PLOS ONE 8 (2), e57088.
Efron, B., 1979. Bootstrap methods: another look at the jackknife. Ann. Statist. 7 (1), 1–26. http://dx.doi.org/10.1214/aos/1176344552.
Falconer, M., Gilbert, J., Roper, A., Greenberg, H., Gavora, J., 1995. Rotavirus-induced fusion from without in tissue-culture cells. J. Virol. 69 (9), 5582–5591.
Fleming, F.E., Graham, K.L., Takada, Y., Coulson, B.S., 2011. Determinants of the specificity of rotavirus interactions with the alpha 2 beta 1 integrin. J. Biol. Chem. 286 (8), 6165–6174. http://dx.doi.org/10.1074/jbc.M110.142992.
Galan, N.O., Rubiano, J.U., Reyes, F.V., Duarte, K.F., Cardenas, S.S., Fernandez, M.G., 2016. In vitro antiviral activity of lactobacillus casei and bifidobacterium adolescentis against rotavirus infection monitored by NSP4 protein production. J. App.. Microbiol. 120, 1041–1051. http://dx.doi.org/10.1111/jam.13069.
Gelberg, H., Hall, W., Woode, G., Basgall, E., Scher, G., 1990. Multinucleate enterocytes associated with experimental group A porcine rotavirus infection. Vet. Pathol. 27, 453–454.
Gervasi, G., Capanna, A., Mita, V., Zaratti, L., Franco, E., 2016. Nosocomial rotavirus infection: an up to date evaluation of european studies. Human Vac. Immunother. 12 (9), 2413–2418. http://dx.doi.org/10.1080/21645515.2016.1183858.
Gilbert, J., Greenberg, H., 1997. Virus-like particle-induced fusion from without in tissue culture cells: role of outer-layer proteins VP4 and VP7. J. Virol. 71 (6), 4555–4563.
Golberg, D.E., 1989. Genetic Algorithms in Search, Optimization, and Machine Learning. Addison Wesley.
Gonzalez-Parra, G., Dobrovolny, H.M., 2015. Assessing uncertainty in A2 respiratory syncytial virus (RSV) viral dynamics. Comput. Math. Methods Med. 2015, 567589. http://dx.doi.org/10.1155/2015/567589.
Gonzalez-Parra, G., Rodriguez, T., Dobrovolny, H.M., 2016. A comparison of methods for extracting influenza viral titer characteristics. J. Virol. Methods 231, 14–24. http://dx.doi.org/10.1016/j.jviromet.2016.02.005.
Groene, W., Shaw, R., 1992. Psoralen preparation of antigenically intact noninfectious rotavirus particles. J. Virol. Methods 138 (1), 93–102. http://dx.doi.org/10.1016/0166-0934(92)90172-A.
Guerrero, C., Santana, A., Acosta, O., 2010. Mouse intestinal villi as a model system for studies of rotavirus infection. J. Virol. Methods 168, 22–30. http://dx.doi.org/10.1016/j.jviromet.2010.04.010.
Guerrero, C.A., Pardo, P., Rodriguez, V., Guerrero, R., Acosta, O., 2013. Inhibition of rotavirus ECWT infection in ICR suckling mice by n-acetylcysteine, peroxisome proliferator-activated receptor gamma agonists and cyclooxygenase-2 inhibitors. Mem. Inst. Oswaldo Cruz 108 (6), 741–754.
Guerrero, C.A., Torres, D.P., García, L.L., Guerrero, R.A., Acosta, O., 2014. N-acetylcysteine treatment of rotavirus-associated diarrhea in children. Pharmacotherapy 34 (11), e333–e340.
Guerrero, C.A., Guerrero, R.A., Silva, E., Acosta, O., Barreto, E., 2016. Experimental adaptation of rotaviruses to tumor cell lines. PLOS ONE 11 (2), e0147666. http://dx.doi.org/10.1371/journal.pone.0147666.
Heider, S., Metzner, C., 2014. Quantitative real-time single particle analysis of virions. Virology 462, 199–206. http://dx.doi.org/10.1016/j.virol.2014.06.005.
Ho, M., Glass, R., Pinsky, P., Anderson, L., 1988. Rotavirus as a cause of diarrheal morbidity and mortality in the united states. J. Infect. Dis. 158 (5), 1112–1116.

Holder, B.P., Beauchemin, C.A., 2011. Exploring the effect of biological delays in kinetic models of influenza within a host or cell culture. BMC Public Health 11 (S1), S10. http://dx.doi.org/10.1186/1471-2458-11-S1-S10.
Holland, J.H., 1992. Genetic algorithms. Sci. Am. 267 (1), 66–72.
Holloway, G., Coulson, B.S., 2013. Innate cellular responses to rotavirus infection. J. Gen. Virol. 94 (6), 1151–1160. http://dx.doi.org/10.1099/vir.0.051276-0.
Huang, F., Wang, B.-R., Wu, Y.-Q., Wang, F.-C., Zhang, J., Wang, Y.-G., 2016. Oncolytic viruses against cancer stem cells: a promising approach for gastrointestinal cancer. World J. Gastroenterol. 22 (35), 7999–8009.
Kaljot, K.T., Shaw, R.D., Rubin, D.H., Greenberg, H.B., 1988. Infectious rotavirus enters cells by direct cell membrane penetration, not by endocytosis. J. Virol. 62 (4), 1136–1144.
Kang, J.Y., Lee, D.K., Ha, N.J., Shin, H.S., 2015. Antiviral effects of lactobacillus ruminis SPM0211 and bifidobacterium longum SPM1205 and SPM1206 on rotavirus-infected Caco-2 cells and a neonatal mouse model. J. Microbiol. 53 (11), 796–803. http://dx.doi.org/10.1007/s12275-015-5302-2.
Kitamoto, N., Ramig, R.F., Matson, D.O., Estes, M.K., 1991. Comparative growth of different rotavirus strains in differentiated cells (MA104, HepG2, and CaCo-2). Virology 184, 729–737.
Knipping, K., Garssen, J., van't Land, B., 2012. An evaluation of the inhibitory effects against rotavirus infection of edible plant extracts. Virol. J. 9 (1), 1–8.
Kreutz, C., Raue, A., Timmer, J., 2012. Likelihood based observability analysis and confidence intervals for predictions of dynamic models BMC Syst. Biol. 1, 120.
Lamberti, L.M., Ashraf, S., Walker, C.L.F., Black, R.E., 2016. A systematic review of the effect of rotavirus vaccination on diarrhea outcomes among children younger than 5 years. Ped. Infect. Dis. J. 35 (9), 992–998.
Lee, D.K., Park, J.E., Kim, M.J., Seo, J.G., Lee, J.H., Ha, N.J., 2015. Probiotic bacteria, *B. longum* and *L. acidophilus* inhibit infection by rotavirus in vitro and decrease the duration of diarrhea in pediatric patients. Clin. Res. Hepatol. Gastroenterol. 39 (2), 237–244. http://dx.doi.org/10.1016/j.clinre.2014.09.00.
Lopez, T., Lopez, S., Arias, C.F., 2015. The tyrosine kinase inhibitor genistein induces the detachment of rotavirus particles from the cell surface. Virus Res. 210, 141–148. http://dx.doi.org/10.1016/j.virusres.2015.07.020.
Lopman, B.A., Pitzer, V.E., Sarkar, R., Gladstone, B., Patel, M., Glasser, J., Gambhir, M., Atchison, C., Grenfell, B.T., Edmunds, W.J., Kang, G., Parashar, U.D., 2012. Understanding reduced rotavirus vaccine efficacy in low socio-economic settings. PLoS ONE 7 (8), e41720. http://dx.doi.org/10.1371/journal.pone.0041720.
Makabe, T., Sato, M., Ouneda, S., Inaba, Y., 1986. Hemagglutination with ovine rotavirus. Arch. Virol. 90, 153–158.
Mehendale, S., Venkatasubramanian, S., Kumar, C.G., Kang, G., Gupte, M., Arora, R., 2016. Expanded Indian national rotavirus surveillance network in the context of rotavirus vaccine introduction. Indian Pediatr. 53 (7), 575–581. http://dx.doi.org/10.1007/s13312-016-0891-3.
Morelli, M., Ogden, K.M., Patton, J.T., 2015. Silencing the alarms: Innate immune antagonism by rotavirus NSP1 and VP3. Virology 479 (SI), 75–84. http://dx.doi.org/10.1016/j.virol.2015.01.006.
Nayyar, M., Cheng, P., Desai, B., Cen, S., Desai, M., Gill, I., Duddalwar, V., 2016. Active surveillance of small renal masses: a review on the role of imaging with a focus on growth rate. J. Comput. Assist. Tomogr. 40 (4), 517–523. http://dx.doi.org/10.1097/RCT.0000000000000407.
Neumann, A.U., Lam, N.P., Dahari, H., Gretch, D.R., Wiley, T.E., Layden, T.J., Perelson, A.S., 1998. Hepatitis C viral dynamics in vivo and the antiviral efficacy of interferon-α therapy. Science 282 (5386), 103–107.
Nguyen, V.K., Binder, S.C., Boianelli, A., Meyer-Hermann, M., Hernandez-Vargas, E.A., 2015. Ebola virus infection modeling and identifiability problems. Front. Microbiol. 6, 257. http://dx.doi.org/10.3389/fmicb.2015.00257.
Nguyen, V.K., Klawonn, F., Mikolajczyk, R., Hernandez-Vargas, E.A., 2016. Analysis of practical identifiability of a viral infection model. PLOS ONE 11 (12), e0167568.
Omondi, O.L., Wang, C., Xue, X., Lawi, O.G., 2015. Modeling the effects of vaccination on rotavirus infection. Adv. Difference Equ. 381. http://dx.doi.org/10.1186/s13662-015-0722-1.
Padhi, R., Bhardhwaj, J.R., 2009. An adaptive drug delivery design using neural networks for effective treatment of infectious diseases: a simulation study. Comput. Methods Programs Biomed. 94 (3), 207–222.
Paradis, E.G., Pinilla, L.T., Holder, B.P., Abed, Y., Boivin, G., Beauchemin, C.A.A., 2015. Impact of the H275Y and I223V mutations in the neuraminidase of the 2009 pandemic influenza virus in vitro and evaluating experimental reproducibility. PLOS ONE 10 (5), e0126115. http://dx.doi.org/10.1371/journal.pone.0126115.
Pawelek, K.A., Huynh, G.T., Quinlivan, M., Cullinane, A., Rong, L., Perelson, A.S., 2012. Modeling within-host dynamics of influenza virus infection including immune responses. PLoS Comput. Biol. 8 (6), e1002588. http://dx.doi.org/10.1371/journal.pcbi.1002588.
Perelson, A.S., Neumann, Markowitz, M., Leonard, J., Ho, D., 1996. HIV-1 dynamics in vivo: virion clearance rate, infected cell life-span, and viral generation time. Sci. 5255, 1582–1586.
Pinilla, L.T., Holder, B.P., Abed, Y., Boivin, G., Beauchemin, C.A.A., 2012. The H275Y neuraminidase mutation of the pandemic A/H1N1 influenza virus lengthens the eclipse phase and reduces viral output of infected cells, potentially compromising fitness in ferrets. J. Virol. 86 (19), 10651–10660. http://dx.doi.org/10.1128/?JVI.07244-11.
Pitzer, V.E., Patel, M.M., Lopman, B.A., Viboud, C., Parashar, U.D., Grenfell, B.T., 2011. Modeling rotavirus strain dynamics in developed countries to understand the potential impact of vaccination on genotype distributions. Proc. Natl. Acad. Sci. U.S.A. 108 (48), 19353–19358.
Prelog, M., Gorth, P., Zwazl, I., Kleines, M., Streng, A., Zlamy, M., Heinz-Erian, P., Wiedermann, U., 2016. Universal mass vaccination against rotavirus: indirect effects on rotavirus infections in neonates and unvaccinated young infants not eligible for vaccination. J. Infect. Dis. 214 (4), 546–555. http://dx.doi.org/10.1093/infdis/jiw186.
Press, W.H., Teukolsky, S.A., Vetterling, W.T., Flannery, B.P., 1992. Numerical recipes: the art of scientific computing. Cambridge.
Raue, A., Kreutz, C., Maiwald, T., Bachmann, J., Schilling, M., Klingmüller, U., Timmer, J., 2009. Structural and practical identifiability analysis of partially observed dynamical models by exploiting the profile likelihood. Bioinformatics 25 (15), 1923–1929.
Raue, A., Kreutz, C., Theis, F.J., Timmer, J., 2013. Joining forces of Bayesian and frequentist methodology: a study for inference in the presence of non-identifiability. Phil. Trans. R. Soc. A 371 (1984), 20110544.
Santosham, M., 2010. Rotavirus vaccine: a powerful tool to combat deaths from diarrhea. N. Engl. J. Med. 362 (4), 358–360.
Sheikhan, M., Ghoreishi, S., 2013. Antiviral therapy using a fuzzy controller optimized by modified evolutionary algorithms: a comparative study. Neural Comput. Appl. 23 (6), 1801–1813.
Simon, P.F., de La Vega, M.-A., Paradis, É., Mendoza, E., Coombs, K.M., Kobasa, D., Beauchemin, C.A.A., 2016. Avian influenza viruses that cause highly virulent infections in humans exhibit distinct replicative properties in contrast to human H1N1 viruses. Sci. Rep. 6, 24154. http://dx.doi.org/10.1038/srep24154.
Smith, A.M., Adler, F.R., Perelson, A.S., 2010. An accurate two-phase approximate solution to an acute viral infection model. J. Math. Biol. 60 (5), 711–726. http://dx.doi.org/10.1007/s00285-009-0281-8.
Suzuki, H., Kitaoka, S., Konno, T., Sato, T., Ishida, N., 1985. Two modes of human rotavirus entry into MA104 cells. Arch. Virol. 85 (1-2), 25–34.
Tönsing, C., Timmer, J., Kreutz, C., 2017. Profile likelihood based analyses of infectious disease models. Stat. Methods Med. Res (in press).
Wu, H., Zhu, H., Miao, H., Perelson, A.S., 2008. Parameter identifiability and estimation of HIV/AIDS dynamic models. Bull. Math. Biol. 70 (3), 785–799.
Yin, Y., Bijvelds, M., Dang, W., Xu, L., van der Eijk, A.A., Knipping, K., Tuysuz, N., Dekkers, J.F., Wang, Y., de Jonge, J., Sprengers, D., van der Laan, L.J., Beekman, J.M., ten Berge, D., Metselaar, H.J., de Jonge, H., Koopmans, M.P., Peppelenbosch, M.P., Pan, Q., 2015. Modeling rotavirus infection and antiviral therapy using primary intestinal organoids. Antiviral Res. 123, 120–131. http://dx.doi.org/10.1016/j.antiviral.2015.09.010.
Zhang, L., Peeples, M.E., Boucher, R.C., Collins, P.L., Pickles, R.J., 2002. Respiratory syncytial virus infection of human airway epithelial cells is polarized, specific to ciliated cells, and without obvious cytopathology. J. Virol. 76 (11), 5654–5666. http://dx.doi.org/10.1128/JVI.76.11. 5654-5666.2002.
Zhao, X., Chester, C., Rajasekaran, N., He, Z., Kohrt, H.E., 2016. Strategic combinations: the future of oncolytic virotherapy with reovirus. Mol. Can. Therapeut. 15 (5), 767–773. http://dx.doi.org/10.1158/1535-7163.MCT-15-0695.